



RESEARCH ARTICLE

10.1002/2015PA002820

Key Points:

- A new high-resolution record of the OMT from Site U1334
- Site U1334 stable isotope data represent global deep water signals
- We create a benthic foraminiferal stable isotope stack across the OMT

Supporting Information:

- Texts S1–S3 and Figures S1–S8

Correspondence to:

H. M. Beddow,
h.m.beddow-twig@uu.nl

Citation:

Beddow, H. M., D. Liebrand, A. Sluijs, B. S. Wade, and L. J. Lourens (2016), Global change across the Oligocene-Miocene transition: High-resolution stable isotope records from IODP Site U1334 (equatorial Pacific Ocean), *Paleoceanography*, 31, 81–97, doi:10.1002/2015PA002820.

Received 24 APR 2015

Accepted 3 DEC 2015

Accepted article online 12 DEC 2015

Published online 16 JAN 2016

Global change across the Oligocene-Miocene transition: High-resolution stable isotope records from IODP Site U1334 (equatorial Pacific Ocean)

Helen M. Beddow¹, Diederik Liebrand², Appy Sluijs¹, Bridget S. Wade³, and Lucas J. Lourens¹

¹Department of Earth Sciences, Faculty of Geosciences, Utrecht University, Utrecht, Netherlands, ²Ocean and Earth Science, National Oceanography Centre, University of Southampton, Southampton, UK, ³Department of Earth Sciences, Faculty of Mathematical and Physical Sciences, University College, London, UK

Abstract The Oligocene-Miocene transition (OMT) (~23 Ma) is interpreted as a transient global cooling event, associated with a large-scale Antarctic ice sheet expansion. Here we present a 2.23 Myr long high-resolution (~3 kyr) benthic foraminiferal oxygen and carbon isotope ($\delta^{18}\text{O}$ and $\delta^{13}\text{C}$) record from Integrated Ocean Drilling Program Site U1334 (eastern equatorial Pacific Ocean), covering the interval from 21.91 to 24.14 Ma. To date, five other high-resolution benthic foraminiferal stable isotope stratigraphies across this time interval have been published, showing a ~1‰ increase in benthic foraminiferal $\delta^{18}\text{O}$ across the OMT. However, these records are still few and spatially limited and no clear understanding exists of the global versus local imprints. We show that trends and the amplitudes of change are similar at Site U1334 as in other high-resolution stable isotope records, suggesting that these represent global deep water signals. We create a benthic foraminiferal stable isotope stack across the OMT by combining Site U1334 with records from ODP Sites 926, 929, 1090, 1264, and 1218 to best approximate the global signal. We find that isotopic gradients between sites indicate interbasinal and intrabasinal variabilities in deep water masses and, in particular, note an offset between the equatorial Atlantic and the equatorial Pacific, suggesting that a distinct temperature gradient was present during the OMT between these deep water masses at low latitudes. A convergence in the $\delta^{18}\text{O}$ values between infaunal and epifaunal species occurs between 22.8 and 23.2 Ma, associated with the maximum $\delta^{18}\text{O}$ excursion at the OMT, suggesting climatic changes associated with the OMT had an effect on interspecies offsets of benthic foraminifera. Our data indicate a maximum glacioeustatic sea level change of ~50 m across the OMT.

1. Introduction

The Oligocene-Miocene transition (OMT; ~23 Ma) is characterized by a ~1‰ positive excursion in marine benthic foraminiferal $\delta^{18}\text{O}$ records. This $\delta^{18}\text{O}$ increase is inferred as a large-scale, rapid expansion in ice volume on Antarctica and an accompanied drop in high-latitude and deep ocean temperatures [Woodruff and Savin, 1989; Miller et al., 1991; Zachos et al., 1997]. Across the OMT, the benthic $\delta^{18}\text{O}$ record shifts from relatively low amplitude climate variability in the late Oligocene, toward high-amplitude, rapid climate variability in the early Miocene [Zachos et al., 2001; Billups et al., 2004; Pälike et al., 2006a, 2006b; Liebrand et al., 2011; Holbourn et al., 2015]. The late Oligocene interval is interpreted as a time of relatively warm global temperatures and low Antarctic ice volume, whereas the early Miocene record is thought to reflect large-scale temperature and ice volume fluctuations [e.g., Miller et al., 1991; Zachos et al., 2001; Shevenell and Kennett, 2007; Mawbey and Lear, 2013].

Stable isotope records across the OMT come primarily from Ocean Drilling Program (ODP) sites located in the Atlantic Ocean, whereas the Pacific Ocean is comparatively understudied. While the benthic foraminiferal stable isotope record from Pacific Ocean Site 1218 provided detailed time control of the entire Oligocene, it is less evenly sampled and of lower resolution after the OMT [Lear et al., 2004; Pälike et al., 2006b]. The Pacific Ocean plays a dominant role in the global transport of heat and salt and represents the largest reservoir of carbon in the exogenic carbon pool strongly influencing the global carbon cycle, predominantly through regionally high primary productivity [Lyle et al., 2008]. The Integrated Ocean Drilling Program (IODP) revisited the equatorial Pacific during the Pacific Equatorial Age Transect (PEAT) Expeditions 320/321 to broaden current understanding of Cenozoic climate and carbon cycle history [Lyle et al., 2010]. Here we present a 2.3 Myr high-resolution (3 kyr) benthic foraminiferal stable isotope record from IODP Site U1334,

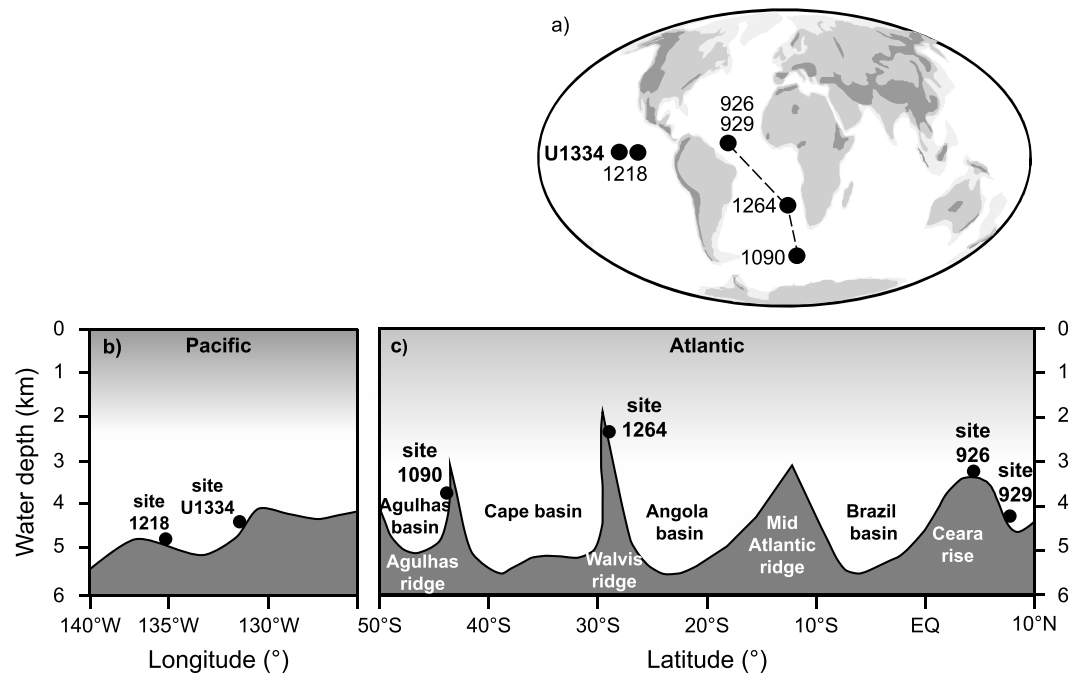


Figure 1. (a) Location of IODP Site U1334 with reference to ODP Sites 1264, 1218, 926, 929, and 1090. Schematic transects indicating location and depth of sites included within this study through (b) the eastern equatorial Pacific and (c) the current equatorial and southern Atlantic Ocean. Black dots indicate drill locations. Transects were constructed using ocean data view (Schlitzer [2010], adapted from Liebrand *et al.* [2011]).

covering the interval 21.91–24.14 Ma, providing a fresh opportunity to study the OMT in the Pacific Ocean, and to compare it on both an intrabasin scale, to Site 1218, and interbasin scale, to sites from the Atlantic Ocean [Zachos *et al.*, 2001; Billups *et al.*, 2004; Pälike *et al.*, 2006a, 2006b; Liebrand *et al.*, 2011]. A well-defined magnetostratigraphy is available for Site U1334 [Channell *et al.*, 2013], which forms the basis of our untuned age model used to evaluate climatic change across the OMT.

2. Site Description

The main objective of PEAT Expeditions 320 and 321 was to recover sediments deposited across the equatorial zone from 56 Ma to the present for the purpose of creating a continuous Pacific “Megasplice,” allowing for focus in high resolution on critical intervals of Cenozoic climatic change [Pälike *et al.*, 2010]. A shallow Paleogene calcite compensation depth (CCD) has made obtaining well-preserved carbonate sediments during this stratigraphic interval challenging; however, IODP Expedition 320 recovered a unique sedimentary archive encompassing most major Cenozoic glaciations, including the OMT. Pelagic clays, nannofossil oozes, and nannofossil chalks of early Miocene to late middle Eocene age, deposited on ~38 Ma old oceanic crust, were recovered from three holes drilled at IODP Site U1334 (7°59.998’N, 131°58.408’W), which is situated 4794 m below sea level (mbsl). Oligocene to Miocene sediments at Site U1334 are primarily made up of nannofossil ooze and chalk [Pälike *et al.*, 2010]. The site is estimated to have been positioned at ~4200 m water depth during the OMT, ~500 m above the CCD [Pälike *et al.*, 2010, 2012]. Within this study, we analyze a section of Site U1334 stretching from 77.74 CSF in hole A (core depth below sea floor, equivalent to meters below sea floor or mbsf) to 104.17 CSF in hole B. On the revised splice of Site U1334 [Westerhold *et al.*, 2012], this section runs from 88.93 CCSF-A (core composite depth below seafloor) (U1334A-9H-3) to 121.29 CCSF-A (U1334B-11H-5). Shipboard data indicate that CaCO₃ concentrations are consistently high within this section, ranging from 74 to 95 wt % [Pälike *et al.*, 2010].

Sites selected for global comparison within this study, with the exception of Site 1218, are located in or near the Atlantic Ocean forming a geographic distribution from the Atlantic sector of the Southern Ocean to the equatorial Atlantic (Figure 1). We compare the composite record from Site U1334 with data from ODP Sites 926 (Hole B, 3598 mbsl) and ODP Site 929 (Hole A, 4358 mbsl), drilled at Ceara Rise in the equatorial western

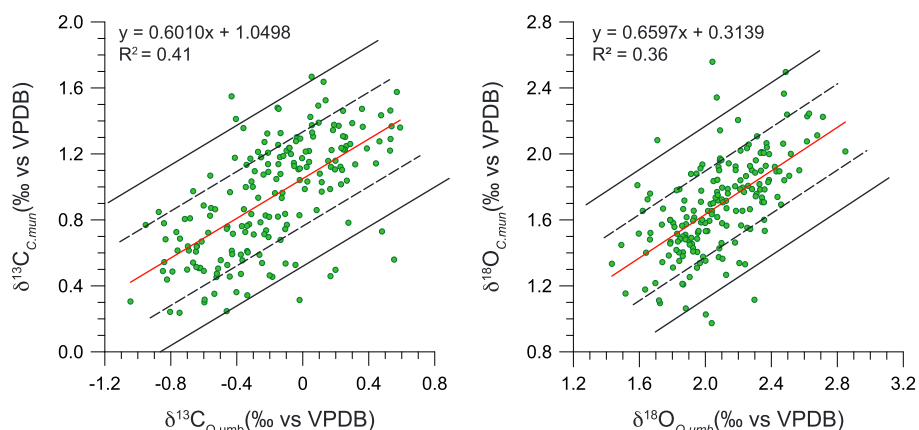


Figure 2. Paired isotope analyses of *Cibicoides mundulus* and *Oridorsalis umbonatus* ($n = 187$). The ordinary least squares regression line is based on the entire data set. The green data points represent data from Site U1334 (this study). The dashed black lines represent 1σ standard deviation (99%), and the solid black lines represent 2σ standard deviation (95%).

Atlantic [Zachos *et al.*, 2001; Pälike *et al.*, 2006a], ODP Site 1090 (composite of Holes D and E, 3699 mbsl) from the Agulhas Ridge in the Atlantic sector of the Southern Ocean [Billups *et al.*, 2004] and ODP Site 1264 (composite of Holes A and B, 2505 mbsl), from the Walvis Ridge in the southeastern Atlantic Ocean [Liebrand *et al.*, 2011]. For a regional equatorial Pacific comparison, we compare our results from Site U1334 with those obtained from ODP Site 1218 (composite of Holes A–C, 4827 mbsl) [Lear *et al.*, 2004; Pälike *et al.*, 2006b], located ~370 km southeast of Site U1334, 28 mbsl deeper than Site U1334 (Figure 1).

3. Methods

The revised splice of Site U1334 [Westerhold *et al.*, 2012] was followed during sampling. Samples of approximately 7.5 cm^3 (quarter core 1 cm slices) of sediment at 4 cm intervals were taken from 88.93 to 121.29 CCSF-A, covering the complete OMT interval. The samples were freeze dried, washed over $38 \mu\text{m}$, $63 \mu\text{m}$, and $150 \mu\text{m}$ sieves, and oven dried at 40°C . Weights were recorded before and after all sample-processing steps. Samples were dry sieved, and two benthic foraminifera species, *Cibicoides mundulus* and *Oridorsalis umbonatus*, were picked from the 250–355 μm size fraction to avoid juvenile specimens with potentially different isotopic compositions, resulting from variability in vital effects between specimens of different age [Schmiedl *et al.*, 2004]. Between 1 and 6 foraminifera were picked, crushed to obtain a homogeneous subsample and ultrasonically cleaned for 2 s while suspended in ethanol. Excess ethanol was pipetted out and the samples dried overnight at 40°C .

Stable isotope analyses were conducted at the Faculty of Geosciences, Utrecht University, using a Thermo-Finnigan Kiel III automated preparation system coupled to a Thermo-Finnigan MAT 253 mass spectrometer. The standard NBS-19 and an in-house marble standard “Naxos” were used to calibrate isotope values to Vienna Pee Dee Belemnite (VPDB). Analytical precision is 0.03‰ and 0.08‰ for $\delta^{13}\text{C}$ and $\delta^{18}\text{O}$, respectively. The standard error derived from running replicate analyses of the samples (15% of the data set) is 0.32‰ and 0.33‰ (Figure S3 in the supporting information). The standard error from the correction factor between the two species is 0.52‰ and 0.45‰ for $\delta^{13}\text{C}$ and $\delta^{18}\text{O}$, respectively. Minimal removal of outliers was performed by eye from both stable isotope data sets; 8 values were removed from the *C. mundulus* data set and 13 values from the *O. umbonatus* data set (Figure S2 in the supporting information).

4. Results

4.1. Interspecies Comparison

Oligocene-Miocene foraminifera present at Site U1334 have moderate to good preservation [Pälike *et al.*, 2010; Edgar *et al.*, 2013]. *Cibicoides mundulus* is present in most samples and is measured within this study as the main species; however, in some samples *C. mundulus* is scarce or even absent. The scarcity is most likely a result of the quarter core sample size and/or reflects overall low epifaunal foraminiferal abundances.

Table 1. Correction Factors

Study	Correction Factor $\delta^{13}\text{C}$	Correction Factor $\delta^{18}\text{O}$
This study	$Cib = (0.60 \times Orid) + 1.05 (\pm 0.10)^a$	$Cib = (0.66 \times Orid) + 0.31 (\pm 0.12)^a$
Shackleton et al. [1984]	+1.0‰	-0.5‰
Katz et al. [2003]	+0.72 ($\pm 0.06\%$) ^a	-0.28 ($\pm 0.06\%$) ^a
Billups et al. [2004]	+1.3 ($\pm 0.37\%$) ^b	-0.4 ($\pm 0.27\%$) ^b
Coxall and Wilson [2011]	+1.3‰	-0.34‰

^aThe uncertainty is 2× the standard error of the mean.

^bThe uncertainty is the standard deviation Cib = *Cibicoides mundulus*. Orid = *Oridorsalis umbonatus*.

Owing to the scarcity of *C. mundulus* we use *Oridorsalis umbonatus* to fill gaps in our *C. mundulus* record and obtain a high-resolution record. Specimens of *O. umbonatus* are ubiquitous at Site U1334 throughout the Oligocene-Miocene interval and are also used in other high-resolution stable isotope records across the OMT [Billups et al., 2004].

We compare pairs of *O. umbonatus* and *C. mundulus* stable isotope values from 187 samples to calculate interspecies offsets across the OMT using an ordinary least squares linear regression (Figure 2). This linear regression implies correction factors of $C. mundulus = (0.60 \times O. umbonatus) + 1.05 (\pm 0.10)$ and $C. mundulus = (0.66 \times O. umbonatus) + 0.31 (\pm 0.12)$ with R^2 values of 0.41 and 0.36 for $\delta^{13}\text{C}$ and $\delta^{18}\text{O}$, respectively. Spearman's rank correlation of the relationship between *C. mundulus* and *O. umbonatus* values from the same sample show a statistically significant relationship (>99%), yielding a coefficient of $\rho = 0.65$ for the $\delta^{13}\text{C}$ values and $\rho = 0.63$ for the $\delta^{18}\text{O}$ values. The 95% confidence interval on the slope of the regression line is ± 0.71 and ± 0.79 for $\delta^{13}\text{C}$ and $\delta^{18}\text{O}$, respectively. The sign of the corrections applied to *O. umbonatus* values is in agreement with previous estimates [Shackleton et al., 1984; Katz et al., 2003; Billups et al., 2004; Coxall and Wilson, 2011] (Table 1, see also Figures S4 and S6 in the supporting information).

After correcting for the offset between the two species, we obtain benthic foraminiferal $\delta^{13}\text{C}$ and $\delta^{18}\text{O}$ composite records for Site U1334 (Figure 3). Although the correlation coefficients between the individual *O. umbonatus* and *C. mundulus* records are low, the offset between *C. mundulus* and *O. umbonatus* appears to be fairly consistent in the depth domain during the late Oligocene and early Miocene, with *O. umbonatus* values on average 0.5‰ higher in $\delta^{18}\text{O}$ and 1.1‰ lower in the $\delta^{13}\text{C}$ than the *C. mundulus* values. The *C. mundulus* $\delta^{18}\text{O}$ values, however, indicate a greater range of variability (0.97–2.71‰), compared to the corrected *O. umbonatus* $\delta^{18}\text{O}$ values (0.90–2.23‰). From ~101 to ~107 CCSF-A, in the $\delta^{18}\text{O}$ record, the offset between the two species is reduced to an average 0.4‰, as *C. mundulus* values shift toward higher $\delta^{18}\text{O}$ values with a greater amplitude than the corresponding *O. umbonatus* values (Figures 3 and 4).

To assess the validity of applying the correction factor shown in Figure 2, we performed a sensitivity study to see how robust the record is and how much trends and variability within the record are affected by potential error introduced by using the correction factor. We applied previously reported correction factors [Shackleton et al., 1984; Katz et al., 2003; Billups et al., 2004; Coxall and Wilson, 2011] to the *O. umbonatus* values from Site U1334, resulting in *O. umbonatus* values with a variability of 0.58‰ for $\delta^{13}\text{C}$ and 0.28‰ for $\delta^{18}\text{O}$. Wavelet analyses on the subsequent records showed virtually identical results, indicating that periodicities of change within the record (and their relative amplitudes with respect to each other) are not sensitive to the correction factor used (Figures S4–S7 in the supporting information).

4.2. Age Model

Site U1334 provides a complete magnetostratigraphy for the OMT interval (Figures 3 and 5) [Channell et al., 2013]. By assigning the most recent GTS2012 [Hilgen et al., 2012; Vandenberghe et al., 2012] polarity chron ages to the magnetic reversals at Site U1334, we fit a third-order polynomial to the 14 depth-to-age magnetostratigraphic tie points, which results in a near-linear depth-to-age conversion (Figure 5). The average sedimentation rate is 14.5 m/Myr, with a maximum rate of 15.2 m/Myr and a minimum rate of 12.8 m/Myr. By fitting a third-order polynomial through the GTS2012 polarity ages, we prevent the introduction of spectral power on higher astronomical frequencies (i.e., >10 cycles/Myr), although it should be taken into consideration that the GTS2012 does consider astronomically tuned ages [Billups et al., 2004; Pälike et al., 2006a] for their age calculations of the paleomagnetic reversals [Hilgen et al., 2012;

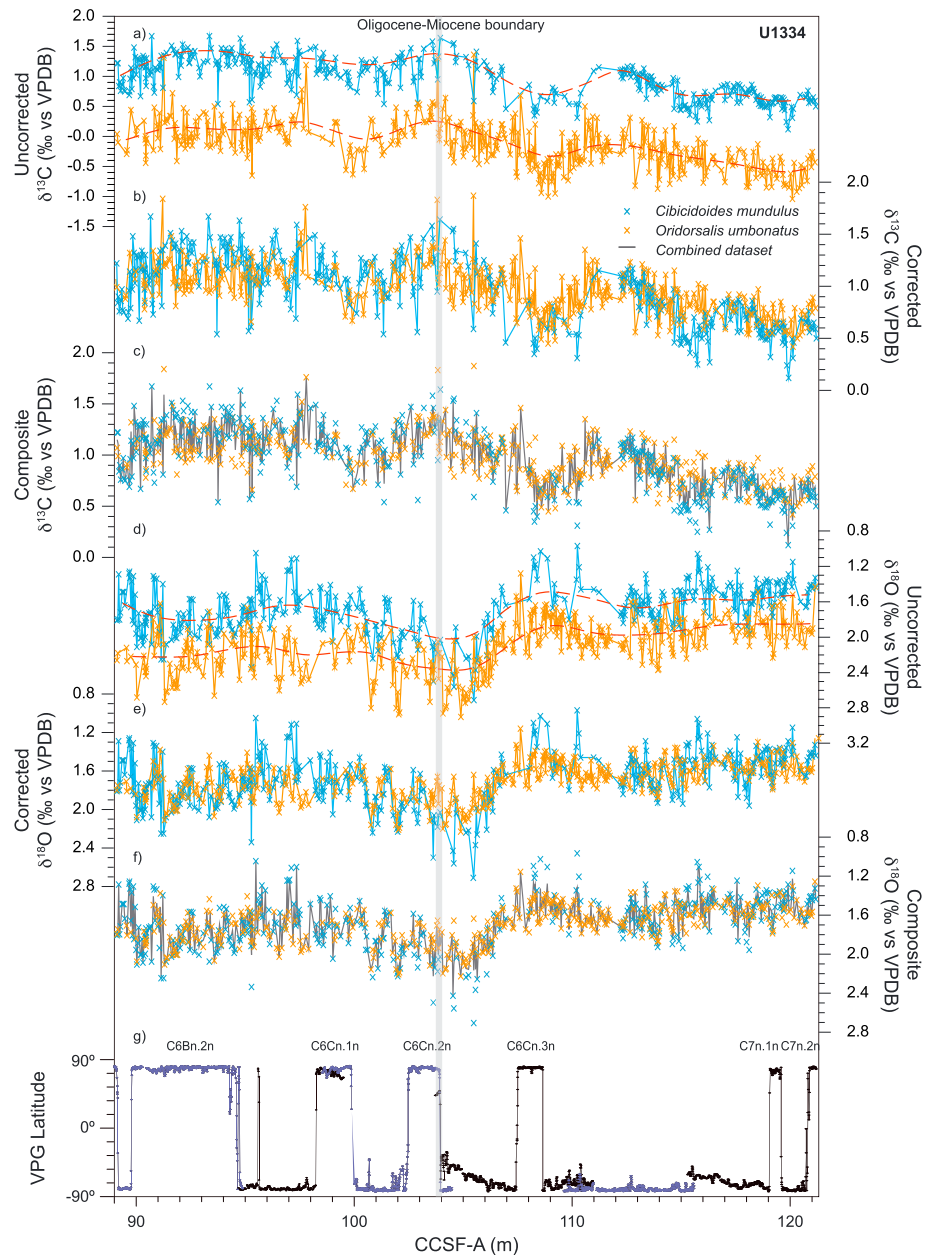


Figure 3. Site U1334 benthic foraminiferal stable isotope records on the CCSF-A depth scale based on the splice by *Westerhold et al.* [2012]. Shown are (a) *Cibicoides mundulus* and uncorrected *Oridorsalis umbonatus* $\delta^{13}\text{C}$ records (red dashed lines indicate long-term SiZer smooths), (b) *C. mundulus* and corrected *O. umbonatus* $\delta^{13}\text{C}$ records, based on the correction factor shown above in Figure 2, (c) the combined composite $\delta^{13}\text{C}$ record used within this study, (d) *Cibicoides mundulus* and uncorrected *Oridorsalis umbonatus* $\delta^{18}\text{O}$ records, (e) *C. mundulus* and corrected *O. umbonatus* $\delta^{18}\text{O}$ records, based on the correction factor shown above in Figure 2, and (f) the combined composite $\delta^{18}\text{O}$ record used within this study. Blue crosses indicate *C. mundulus* values, and orange crosses *O. umbonatus* values. (g) Site U1334 VPG latitudes have been previously published by *Channell et al.* [2013]. Alternate holes are colored blue/black in the VPG latitude plot.

Vandenbergh et al., 2012]. On the magnetostratigraphic age model, our stable isotope records cover the interval 21.91–24.14 Ma with a mean sample resolution of 3.6 kyr (Figure 5).

4.3. Stable Oxygen and Carbon Isotope Composite Records

Within this study, we have chosen to focus on the composite high-resolution two-species data set from Site U1334 (Figure 3), in order to identify and compare trends and patterns present in the Site U1334 data set with

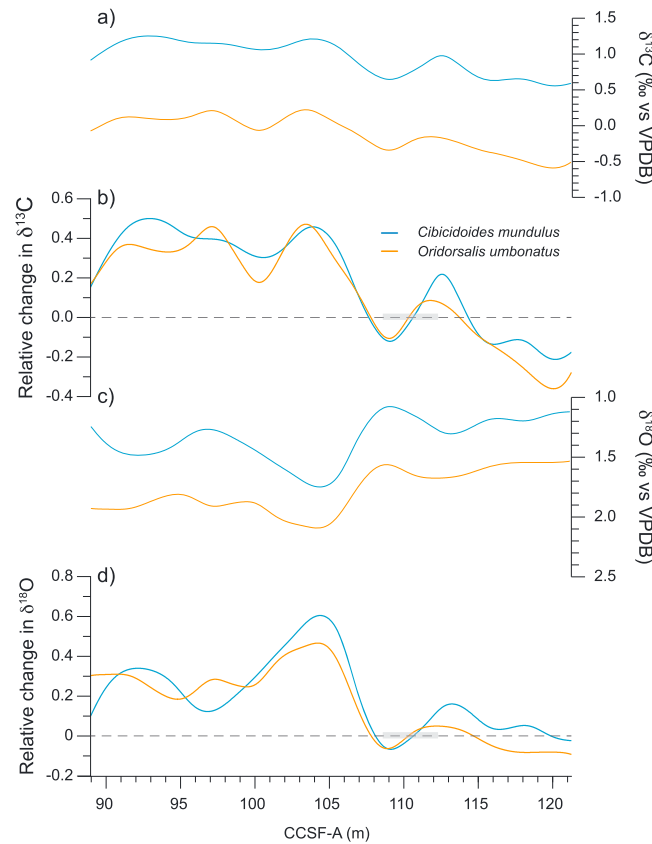


Figure 4. (a) Statistically smoothed *Cibicoides mundulus* and uncorrected *Oridorsalis umbonatus* $\delta^{13}\text{C}$ data sets created using SiZer indicating the long-term (>250 kyr) trend. (b) Relative change in Site U1334 *Cibicoides mundulus* and uncorrected *Oridorsalis umbonatus* $\delta^{13}\text{C}$ data sets based on the long-term SiZer smooths, calculated using a baseline average determined between 108.70 and 112.20 CCSF-A (grey shaded box). (c) Statistically smoothed *Cibicoides mundulus* and uncorrected *Oridorsalis umbonatus* $\delta^{18}\text{O}$ data sets created using SiZer indicating the long-term (>250 kyr) trend. (d) Relative change in Site U1334 *Cibicoides mundulus* and uncorrected *Oridorsalis umbonatus* $\delta^{18}\text{O}$ data sets based on the long-term SiZer smooths, using a baseline average determined between 108.70 and 112.20 CCSF-A (grey shaded box).

other high-resolution stable isotope records across the OMT. Following removal of outliers, the complete record contains 614 values, of which 200 values are *C. mundulus* values, 227 are *O. umbonatus* values corrected to *C. mundulus*, and 187 are values derived from correcting *O. umbonatus* to *C. mundulus*, and then taking an average between the corrected *O. umbonatus* and the *C. mundulus* values. The record using values averaged between the corrected *O. umbonatus* values and *C. mundulus* values has a higher signal to noise ratio than the record constructed using *C. mundulus* values preferentially, with corrected *O. umbonatus* values only present in the data set where no *C. mundulus* data are available. Several peaks in the *C. mundulus* record are not replicated in the *O. umbonatus* record, in particular across the transition. The aim of this paper is to discuss the trends and patterns between records, so we have chosen to use the data set with values averaged between both species for samples where both values are present.

The most prominent feature in the composite stable isotope records is the large positive excursion in the $\delta^{18}\text{O}$ data set, beginning with a steep shift toward more positive values at 23.2 Ma (107.3 CCSF-A) followed by peak positive values (2.43‰) occurring at 23.03 Ma (104.5 CCSF-A)

(Figures 3 and 5). We identify the prominent shift and subsequent recovery as the inception and termination of the OMT. The OMT divides the record into two distinct phases; a period of lower $\delta^{18}\text{O}$ and $\delta^{13}\text{C}$ values with low-amplitude variability ($\sim 0.5\text{‰}$ and $\sim 0.4\text{‰}$ for $\delta^{18}\text{O}$ and $\delta^{13}\text{C}$, respectively) prior to the excursion, from 23.03 to 24.14 Ma (~ 107.3 to 121.3 CCSF-A), and a shift toward more positive values and rapid, high-amplitude variability ($\sim 1.0\text{‰}$ and $\sim 0.6\text{‰}$ for $\delta^{18}\text{O}$ and $\delta^{13}\text{C}$, respectively) after the excursion from 21.91 to 22.9 Ma (~ 88.9 – 102.6 CCSF-A). Variability in the $\delta^{13}\text{C}$ record is noticeably smaller (between 0.1 and 0.4‰) than in the $\delta^{18}\text{O}$ record [Zachos et al., 2001; Pälike et al., 2006a].

4.4. Time Series Analysis

The benthic foraminiferal $\delta^{13}\text{C}$ and $\delta^{18}\text{O}$ time series both exhibit amplitude variability on astronomical frequencies (Figure 6). To illustrate the evolution of astronomical cyclicity through time, we convert our time series into the time-frequency domain using wavelet analyses [Torrence and Compo, 1998] (Figure 6). Prior to analysis, the data were linearly detrended, resampled at a 5 kyr time step and long-term trends (periods longer than 600 kyr) were removed using a Gaussian notch filter, with version 2 of the software package AnalySeries [Paillard et al., 1996]. In addition, we calculate a “family of smooths” on our isotope chronology

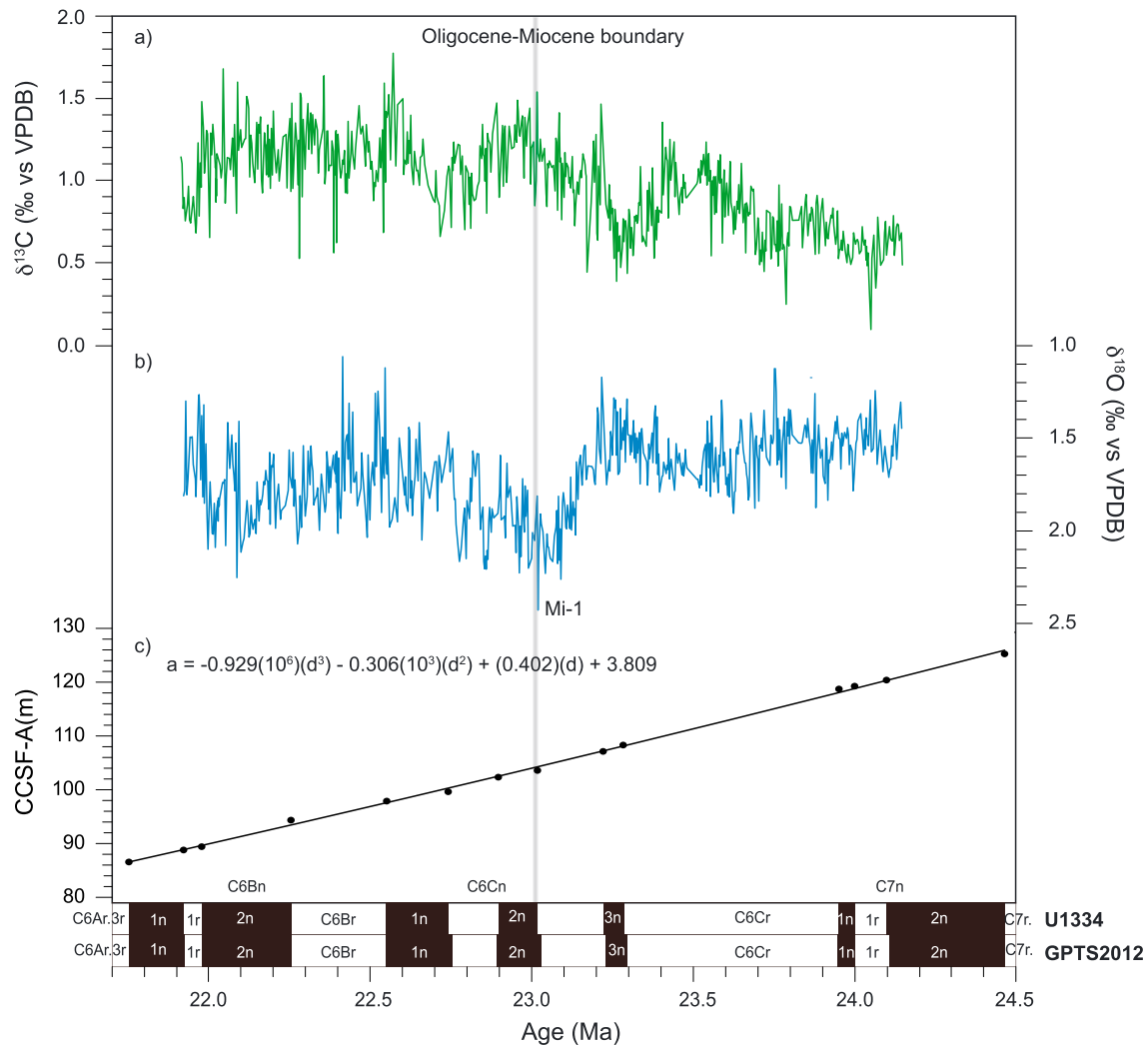


Figure 5. Site U1334 composite benthic foraminiferal stable isotope records of (a) $\delta^{13}\text{C}$ and (b) $\delta^{18}\text{O}$. (c) Magnetic reversal data from Site U1334 placed on the third-order polynomial age model compared to ages published in GTS2012 [Hilgen *et al.*, 2012; Vandenberghe *et al.*, 2012]. The grey shaded line represents the Oligocene/Miocene boundary.

using a space-scale statistical programme SiZer (Significant Zero crossing of derivatives) [Chaudhuri and Marron, 1999], to quantify features in the data set that stand out above the background noise. Of the 41 smooths calculated by SiZer we have selected the 31st and the 24th smooths as they resolve variability on ~100 kyr and >400 kyr timescales, respectively. We will refer to these from this point on in the text as the short-term smooth and long-term smooth. The first set is used to better resolve the orbital components of the records (Figure 6, solid blue line) whereas the second set is used to track climate variability on long-term (>400 kyr) timescales (Figure 6, dashed red line).

Our wavelet analyses show that both isotope records are paced by the long (400 kyr) and short (95–125 kyr) periods of eccentricity, with intervals of obliquity (41 kyr) paced variability (Figure 6). Prior to the inception of the OMT glaciation, long-period eccentricity variability is prominent, particularly in the $\delta^{13}\text{C}$ record, with amplitude variability of 0.4 to 0.8‰. After the termination, both $\delta^{18}\text{O}$ and $\delta^{13}\text{C}$ exhibit increased amplitude variability with typical amplitudes of 0.5 to 1.0‰ on short-term eccentricity frequencies (95–125 kyrs). Significant ~100 kyr and 41 kyr power increases during the OMT and into the early Miocene in both data sets, whereas the 41 kyr signal appears in the wavelet spectrum when the ~100 kyr signal present in the data set is weakest (Figure 6).

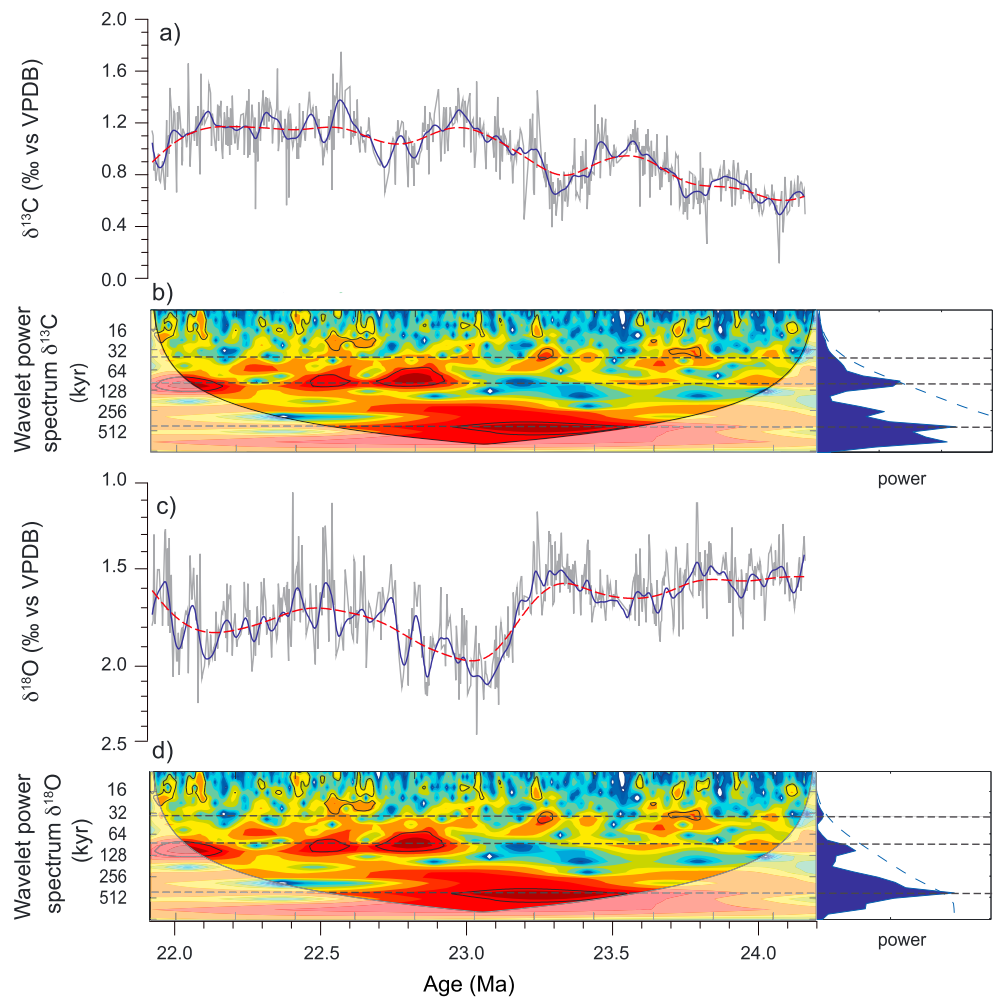


Figure 6. Site U1334 composite benthic foraminiferal stable isotope records of (a) $\delta^{13}\text{C}$ and (c) $\delta^{18}\text{O}$ (c) including two statistical smoothes (blue and dashed red lines) created using SiZer. Wavelet analysis with 95% confidence levels calculated for (b) $\delta^{13}\text{C}$ and (d) $\delta^{18}\text{O}$, calculated using an adapted script from Torrence and Compo [1998]. Data were resampled, notch filtered, and linearly detrended prior to wavelet analysis.

4.5. Global Benthic Stacked Records for $\delta^{13}\text{C}$ and $\delta^{18}\text{O}$ Across the OMT

To create the best approximation of the global isotope signals, we align our data in the depth domain with existing high-resolution benthic foraminiferal stable isotope records from ODP Sites 926, 929, 1090, 1218, and 1264 [Zachos *et al.*, 2001; Billups *et al.*, 2004; Pälike *et al.*, 2006a, 2006b; Liebrand *et al.*, 2011] and create a benthic stack across the OMT. We first correlate the records in the depth domain to Site U1334 using a minimal number of manually selected correlation points and subsequent automated alignment through the application of the Match software package [Lisiecki and Lisiecki, 2002] (supporting information). In addition, we utilized an existing correlation of physical property data from the Pacific Sites 1218 and U1334 [Westerhold *et al.*, 2012]. After all records have been placed on the Site U1334 CCSF-A depth scale, we assigned the ages of our magnetostratigraphic age model to all records. The resulting time series for each site allows the comparison of the available magnetostratigraphies, Site 1218 [Lanci *et al.*, 2004, 2005; Pälike *et al.*, 2006b], Site 1090 [Channell *et al.*, 2003; Billups *et al.*, 2004], and Site 1265 [Bowles, 2006], with that of Site U1334 [Channell *et al.*, 2013] along a common age scale. At Site 1264, no reliable magnetostratigraphy was recovered, so the magnetostratigraphic data from nearby ODP Site 1265 (3083 mbsl) were transferred by pattern matching magnetic susceptibility and color reflectance records [Liebrand *et al.*, 2011]. All reversals, in particular the base of Subchron C6Cn.2n, marking the base of the Miocene, are clearly consistent with the magnetostratigraphies from Sites 1218, 1090, and 1265 (Figures 7 and 8).

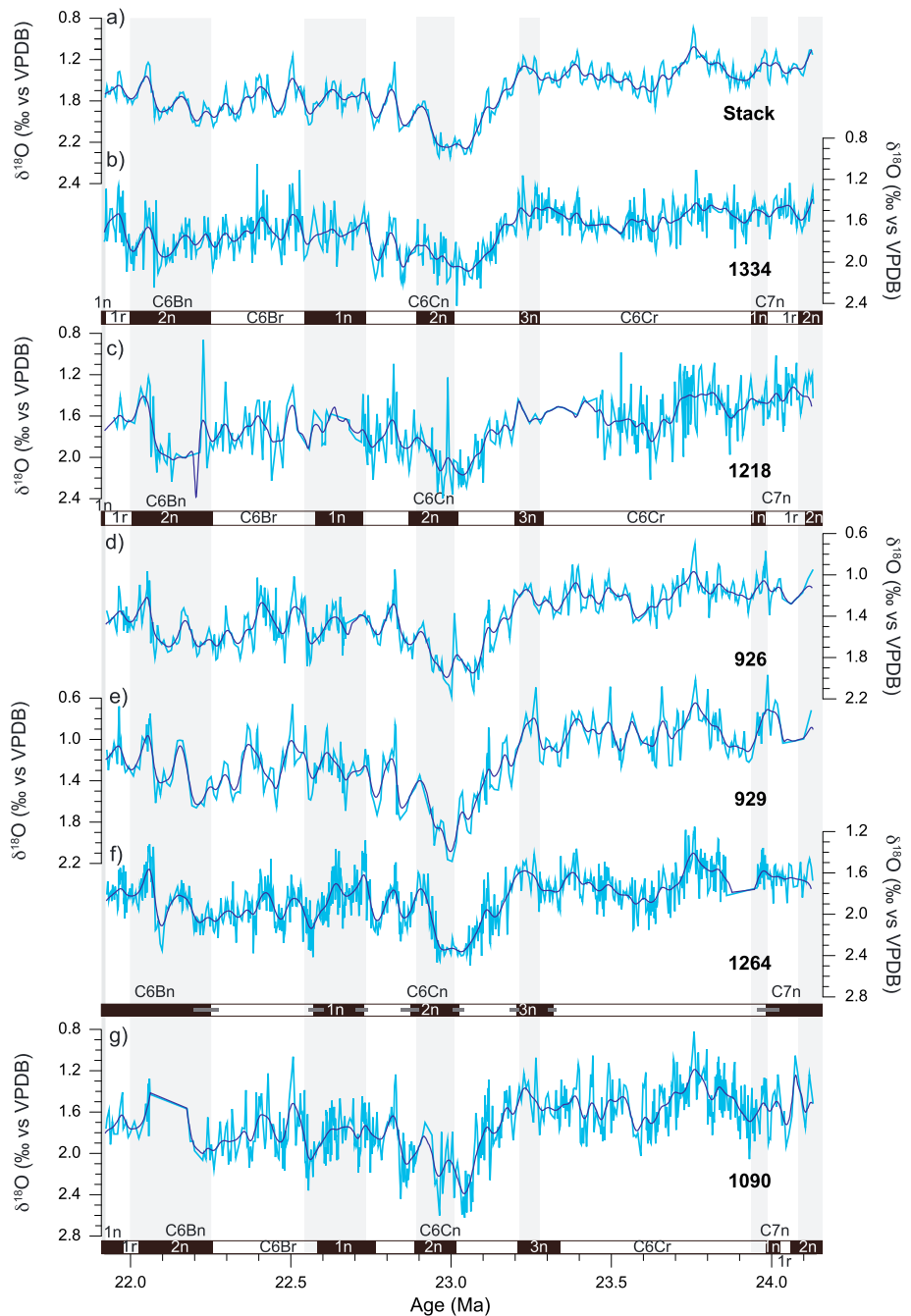


Figure 7. Comparison of Site U1334 with previously published high-resolution benthic foraminiferal $\delta^{18}\text{O}$ records, with magnetic reversal data plotted underneath, adjusted to Site U1334 age model. Dark blue lines are a statistical smooth created using SiZer. Plotted above is (a) the benthic foraminiferal isotope stack, (b) IODP Site U1334 [Channell et al., 2013], (c) ODP Site 1218 [Lanci et al., 2004; Lear et al., 2004; Pälike et al., 2006b], ODP Sites (d) 926 and (e) 929 [Flower et al., 1997; Zachos et al., 1997, 2001; Paul et al., 2000; Pälike et al., 2006a; Shackleton et al., 2000], (f) Site 1264 [Liebrand et al., 2011], and (g) Site 1090 [Channell et al., 2003; Billups et al., 2002, 2004]. The magnetostatigraphy for Site 1264 is transferred from Site 1265 [Bowles, 2006]. The data sets have been aligned at depth using the Match software package [Lisiecki and Lisiecki, 2002] (supporting information) and all data sets then placed on the Site U1334 magnetostratigraphic age model.

As reference for our comparison, we have constructed a composite global stack across the OMT by averaging the benthic foraminiferal stable isotope records of IODP Site U1334 and ODP Sites 926, 929, 1090, 1218, and 1264. Sites 926, 929, 1218, and 1264 are constructed using *Cibicides* spp., and Sites U1334 and 1090 are constructed using both *Cibicides* spp. and *O. umbonatus* corrected to *C. mundulus*. No corrections are

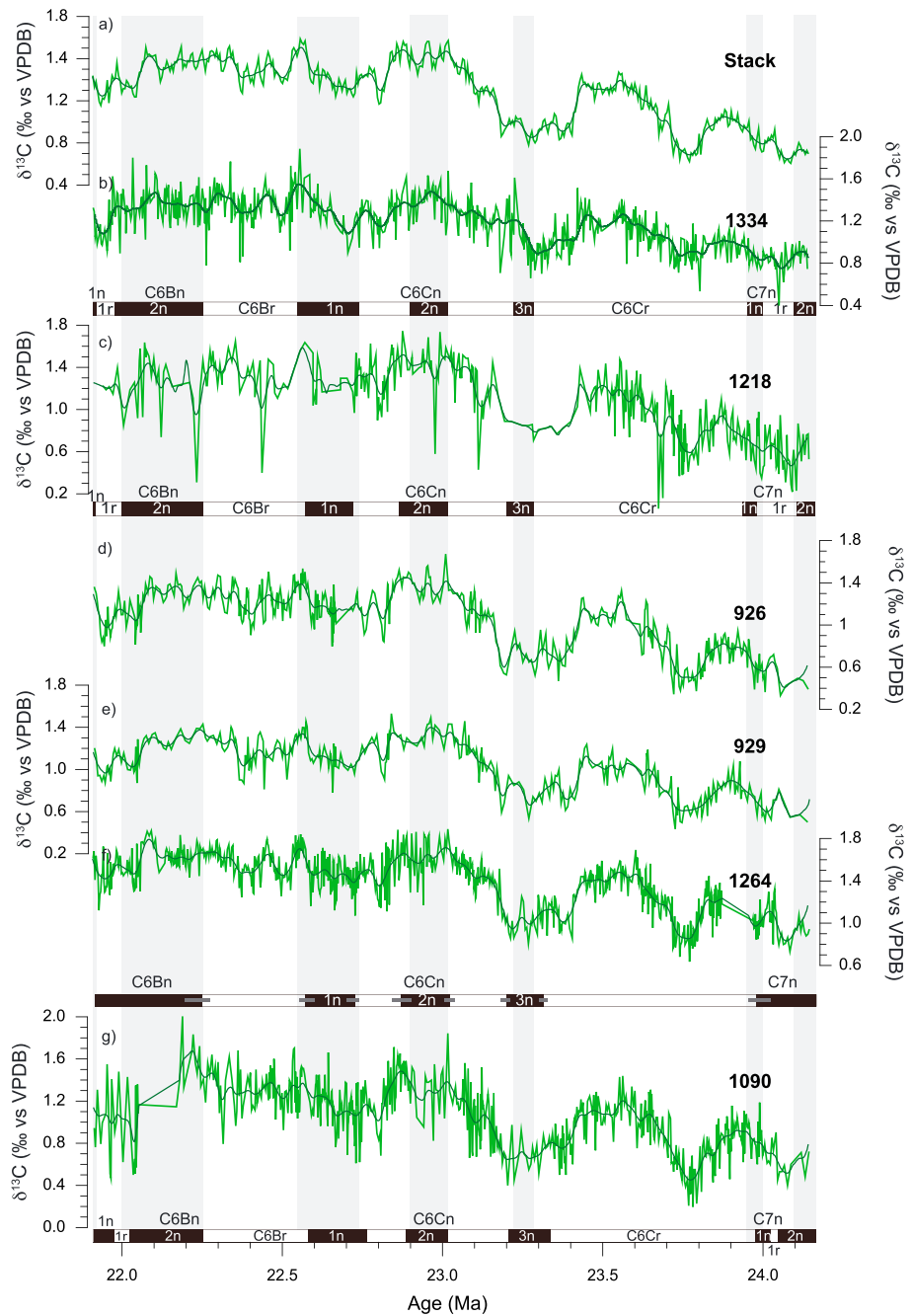


Figure 8. Comparison of Site U1334 with previously published high-resolution benthic foraminiferal $\delta^{13}\text{C}$ records, with magnetic reversal data plotted underneath, adjusted to Site U1334 age model. Dark green lines are a statistical smooth created using SiZer. Plotted above is (a) the benthic foraminiferal stable isotope stack, (b) IODP Site U1334 [Channell *et al.*, 2013], (c) ODP Site 1218 [Lanci *et al.*, 2004; Lear *et al.*, 2004; Pälike *et al.*, 2006b], ODP Sites (d) 926 and (e) 929 [Flower *et al.*, 1997; Zachos *et al.*, 1997, 2001; Paul *et al.*, 2000; Pälike *et al.*, 2006a; Shackleton *et al.*, 2000], (f) Site 1264 [Liebrand *et al.*, 2011], and (g) Site 1090 [Channell *et al.*, 2003; Billups *et al.*, 2002, 2004]. The data sets have been aligned at depth using the Match software package [Lisiecki and Lisiecki, 2002] (supporting information) and all data sets then placed on the Site U1334 magnetostratigraphic age model.

applied for species offsets between records when constructing the stacked record. All analyzed records have a sampling resolution of <10 kyrs. The composite stable isotope stack is created by resampling each record at 5 kyr intervals using AnalySeries, to approximate the true sampling resolution (i.e., not under sample) of the best resolved records and subsequently calculating an equal-weighted average of the six aligned $\delta^{18}\text{O}$ and $\delta^{13}\text{C}$

records. The maximum value in the $\delta^{18}\text{O}$ stack is 2.21‰, and the minimum is 1.79‰ (Figure 7). In the $\delta^{13}\text{C}$ stack, the maxima and minima are 1.89‰ and 0.52‰, respectively (Figure 8). The stacked record captures the full extent of the $\sim 1\%$ shift that occurs in the benthic $\delta^{18}\text{O}$ signal across the OMT. Although the sites used are few, and spatially limited (no data from the North Atlantic and only one fully high-resolution site from the Pacific), the stack is the best global averaged stable isotope signal across the OMT currently possible.

5. Discussion

The benthic foraminiferal $\delta^{18}\text{O}$ signal is a function of the isotopic composition of local seawater $\delta^{18}\text{O}$ and water temperature at the site of calcification. Consistency in both shape and amplitude between the six records across the OMT indicates a true global signal present in the records from Site U1334. Deconvolving the benthic foraminiferal $\delta^{18}\text{O}$ signal into separate components driven by ice volume changes and temperature requires other independent temperature proxies, such as Mg/Ca [Lear *et al.*, 2004; Mawbey and Lear, 2013] or inverse modeling techniques, including ice sheet models for the loci of significant land ice in both hemispheres [De Boer *et al.*, 2010, 2012]. These studies indicate that 50% or more of the benthic $\delta^{18}\text{O}$ signal is driven by changes in Antarctic ice volume. This equates to an average sea level fall of 50 m or more according to a combined benthic $\delta^{18}\text{O}$ and Mg/Ca study of Site 926 records [Mawbey and Lear, 2013] and estimates of 35–40 m based on inverse modeling of benthic $\delta^{18}\text{O}$ from Site 1264 [Liebrand *et al.*, 2011].

5.1. Changes in $\delta^{18}\text{O}$ Offset Between Infaunal and Epifaunal Species at Site U1334

We recognize that the use of two species that exhibit different paleoecological habitats, i.e., epifaunal (*C. mundulus*) and shallow infaunal (*O. umbonatus*), as done within this study and that of Site 1090 [Billups *et al.*, 2004], may influence amplitude variability in the benthic stable isotope records. This may, in turn, complicate the interpretation of the short-term variability in the water masses and climates investigated. In particular, we found a reduction in the $\delta^{18}\text{O}$ offset between *C. mundulus* and *O. umbonatus* occurring within the interval between 108.70 and 112.20 CCSF-A (~ 22.8 – 23.2 Ma), coincident with the positive $\delta^{18}\text{O}$ excursion present at the OMT as reflected in both single species records (Figure 3). The deviation is caused by a larger shift in *C. mundulus* values (epifaunal) (1.1‰) than in *O. umbonatus* values (infaunal) (1.0‰) across the glacial interval. The reduction in the offset between the two species is clear in $\delta^{18}\text{O}$ but minimal in the $\delta^{13}\text{C}$ record, and we find greater variation in $\delta^{18}\text{O}$ interspecies offsets.

We compare the relative change in amplitude across the OMT in the *Cibicidoides mundulus* and uncorrected *Oridorsalis umbonatus* $\delta^{13}\text{C}$ and $\delta^{18}\text{O}$ data sets, calculated by using the long-term SiZer smooths (Figure 3) and a baseline average determined between 108.70 and 112.20 CCSF-A (Figure 4). We find that both $\delta^{13}\text{C}$ data sets have a similar relative change in amplitude across the OMT, but in the *C. mundulus* $\delta^{18}\text{O}$ data set the OMT has a relative amplitude of $\sim 0.6\%$, and the *O. umbonatus* data set has a smaller relative amplitude of $\sim 0.4\%$.

We note a similar reduction in interspecies $\delta^{18}\text{O}$ gradients between *C. mundulus* and *O. umbonatus* occurred across the Eocene-Oligocene boundary at Pacific Site 1218, during a positive shift in $\delta^{18}\text{O}$ associated with the inception of permanent ice sheets on Antarctica [Coxall and Wilson, 2011]. Although it is a very different setting, changes in offsets between the two species have also been noted across the Last Glacial Maximum (LGM) [Thornalley *et al.*, 2015], suggesting that these offsets relate to glacial maxima.

Offsets in stable isotope signals between different benthic foraminifera species are often attributed to differences in metabolic fractionation or “vital effects.” Fluctuations in stable isotope offsets between epifaunal and infaunal species are associated with changes in deep water oxygenation, organic matter fluxes, and pore water DIC concentration, and vertical microhabitat shifts [McConnaughey, 1989a, 1989b; McConnaughey *et al.*, 1997; Schmiedl *et al.*, 2004]. The $\delta^{18}\text{O}$ offset between *C. mundulus* and *O. umbonatus* is not constant through time, and the reduced offset present between 101 and 107 CCSF-A (Figure 3) and could reflect a carbonate ion effect on the benthic $\delta^{18}\text{O}$ isotope signal during the OMT, where a decrease in pH could lead to the $\delta^{18}\text{O}$ of foraminiferal shells becoming isotopically heavier [Zeebe, 1999]. Many studies focus on the implications of the carbonate ion effect for trace metals, suggesting *O. umbonatus* is a reliable species for Mg/Ca and other trace metal species by reasoning that, as an infaunal species, it is protected from fluctuations in the CCD by a buffering effect [Elderfield *et al.*, 2010; Brown *et al.*, 2011; Mawbey and Lear, 2013]; however, few studies have considered the influence of the carbonate ion effect on benthic stable isotopes. A study of the carbonate ion

effect across the Paleocene-Eocene Thermal Maximum suggests that increases in pH across climate transitions could potentially dampen the magnitude of climate excursions recorded in benthic stable isotope signals [Uchikawa and Zeebe, 2010]. Culture studies [e.g., Diz et al., 2012], however, suggest that the carbonate ion effect affects $\delta^{18}\text{O}$ to a much lesser extent than $\delta^{13}\text{C}$, and as our offset in $\delta^{13}\text{C}$ is consistent across the OMT, an alternative mechanism may be controlling the change in interspecies offsets across the OMT.

Fluctuations in $\delta^{18}\text{O}$ interspecies offsets could be indicative of variations in carbonate ion concentration or early diagenetic processes [Schmiedl and Mackensen, 2006; Hoogakker et al., 2010] associated with the shift in climate across the OMT at Site U1334. This suggests that a change in the relationship between the $\delta^{18}\text{O}$ values of infaunal species *O. umbonatus* and the epifaunal species *C. mundulus* is linked to the climatic changes occurring during the positive $\delta^{18}\text{O}$ excursion, notably deep water cooling. However, few data exist on the impact of glacial-interglacial changes on species offsets in benthic foraminiferal stable isotope signals in deep sea cores or on multispecies records from the same cores extending beyond the LGM [Schmiedl and Mackensen, 2006; Friedrich et al., 2006; Hoogakker et al., 2010], making it difficult to pinpoint mechanisms controlling Cenozoic changes in the $\delta^{18}\text{O}$ gradient between benthic foraminiferal species.

5.2. Interbasin Comparison of the OMT

All Pacific and Atlantic high-resolution records throughout the OMT interval show a notable similarity in the shape and amplitude of large- and small-scale features in the data sets and short-term and long-term smooths created using SiZer (Figures 7 and 8). As changes in ice volume should have an equal effect on the $\delta^{18}\text{O}$ of all water masses, the global signal in the $\delta^{18}\text{O}$ records should be comparable, with differences in $\delta^{18}\text{O}$ between records implying a change in deep ocean circulation patterns, regional changes in water mass temperature, or changes in the relationship between salinity and $\delta^{18}\text{O}$, taking offsets between labs (which can be up to 0.2‰) into account [Ostermann and Currie, 2002]. All six records exhibit peak positive $\delta^{18}\text{O}$ values that are often referred to as the Mi-1 isotope zone, or “Mi-1,” which has been identified previously in a number of OMT records [Miller et al., 1991; Billups et al., 2004; Pálfi et al., 2006b]. The peak positive values (Mi-1) at Site U1334 occur at 23.02 Ma, just prior to Chron C6cn.2n, the marker for the Oligocene/Miocene boundary, making it a late Oligocene event rather than a Miocene event (Figures 5 and 7).

Absolute (range from maxima to minima) values of the amplitude of the positive $\delta^{18}\text{O}$ excursion at the OMT range between 1.0‰ (Site 1264) and 1.4‰ (Site 1090). We measure the absolute amplitude of the OMT in each record by taking the difference between the minimum value at 23.2 Ma, where the shifts toward more positive $\delta^{18}\text{O}$ values begins, and the maximum value during the OMT at ~23.0 Ma. One factor to consider with regards to measuring the amplitude of an event using absolute values is that picking a precise point at which the transition starts can be arbitrary and choosing different points in the data set to define the beginning of a transition can lead to different estimates for the absolute amplitude of the event [Mudelsee et al., 2014]. We use the short- and long-term SiZer smooths to distinguish the underlying structure of the data set from the background noise, to pinpoint the beginning of the positive $\delta^{18}\text{O}$ shift at the OMT, and to compare the relative amplitude change during the glaciation between records [Bohaty et al., 2012]. Focusing on differences in the amplitude of the isotope excursion during the OMT using statistically smoothed SiZer data avoids putting too much emphasis on extreme stable isotope values, which might lead to an overestimation or underestimation of differences in amplitude between sites [Mudelsee et al., 2014].

Site 1090 has the largest absolute amplitude across the OMT in terms of maximum and minimum individual $\delta^{18}\text{O}$ values (1.4‰) (Figure 7), but looking at the smoothed data set (Figure 9), equatorial Atlantic Site 929 experiences the largest relative change across the OMT. The relative change in $\delta^{18}\text{O}$ at Site 929 across the OMT is 0.85‰, relative to a baseline determined by averaging $\delta^{18}\text{O}$ values between 23.30 and 23.55 Ma. This is 0.2‰ larger than the relative change at Site 926, which is located near to but 760 m shallower than Site 929. Site 1090 has a relative change in $\delta^{18}\text{O}$ of 0.6‰, and Sites 1218, 1264, and U1334 all have a relative change of 0.5‰. Comparing the relative amplitude of the sites indicates that the equatorial Atlantic sites experienced the largest change in $\delta^{18}\text{O}$ values compared to Pacific Sites. Using the long-term SiZer smooth of our stacked record to estimate relative change in $\delta^{18}\text{O}$ across the OMT, we find a value of 0.6‰ (Figure 7), which agrees with a previously published study, which gives the same figure for an overall weighted mean from 15 high- and low-resolution records [Mudelsee et al., 2014]. We note that the small relative amplitude at Site U1334 could be an artifact of the way the record was constructed, as the offset between the two

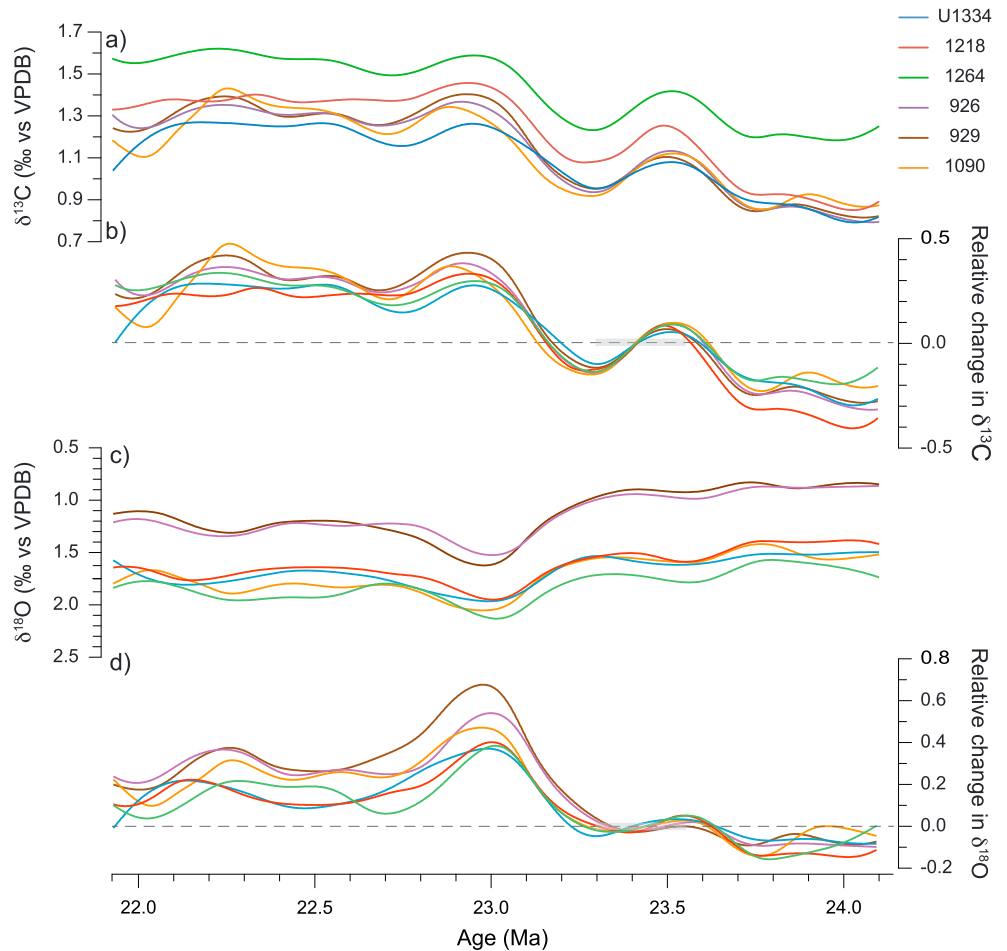


Figure 9. (a) Statistically smoothed $\delta^{18}\text{O}$ data sets from Site U1334 (this study) and previously published data sets from Sites 1218, 926, 929, 1264, and 1090 indicating the long-term (>250 kyr) trend. (b) Relative change in $\delta^{18}\text{O}$ record based on long-term $\delta^{18}\text{O}$ SiZer smooths, using a baseline average determined between 23.3 and 23.5 Ma (grey shaded box). (c) Statistical smoothed $\delta^{13}\text{C}$ data sets from Site U1334 (this study) and previously published data sets from Sites 1218, 926, 929, 1264, and 1090 indicating the long-term (>250 kyr) trend. (d) Relative change in $\delta^{13}\text{C}$ record based on long-term $\delta^{18}\text{O}$ SiZer smooths, using a baseline average determined between 23.3 and 23.5 Ma (grey shaded box).

species is reduced between 22.8 Ma and 23.2 Ma. The 0.5‰ relative change in amplitude in the $\delta^{18}\text{O}$ data set is an average of the *C. mundulus* and *O. umbonatus* data sets. The *C. mundulus* data set has a relative change in amplitude of 0.6‰ (Figure 4), which is in better agreement with the value given by the stacked record and the study from *Mudelsee et al.* [2014]. Comparing relative change in $\delta^{18}\text{O}$ values across the OMT suggests that the upper limit of ice volume change present within the $\delta^{18}\text{O}$ signal across the OMT can be constrained to 0.6‰, which would equate to a maximum ~50 m of sea level fall, assuming an ice sheet $\delta^{18}\text{O}$ identical to today [Fairbanks and Matthews, 1978]. If the $\delta^{18}\text{O}$ of the expanding ice sheet during Mi-1 was higher than today, which can be expected from presumably reduced Rayleigh distillation by atmospheric water transport in a warmer world than the present day, then this estimate could be slightly larger. This would suggest that sea level change across the OMT is in the midrange of previous estimates, which vary from 30 to 90 m [Miller et al., 1991; Pekar et al., 2002; Liebrand et al., 2011; Mawbey and Lear, 2013].

Significant ~100 kyr amplitude variability present in all $\delta^{18}\text{O}$ data sets during the early Miocene suggests short-period eccentricity controlled expansion/contraction of the geographical extent and mass of the Antarctic ice sheet (Figure 6) [Zachos et al., 2001; Liebrand et al., 2011]. Low ~100 kyr amplitude variability during the positive isotope excursion and suggested glacial expansion across the OMT indicates a stable period

of maximum ice volume and persistent low temperatures. More significant ~ 100 kyr variability occurring in the early Miocene is superimposed on a long-term trend in ice sheet decay and relatively higher global temperatures. Strong ~ 100 kyr cyclicity is particularly clear during the termination phase of the transient glaciation across the OMT. All six sites show a clear increase in the amplitude of ~ 100 kyr variability after the termination, although the amplitude of the response differs between basins. In particular, directly after the OMT, three prominent ~ 100 kyr cycles are present in all records but are clearest at Sites U1334 and 1264 (Figures 6 and 7). At 22.7 Ma, Site 1264 has notably high amplitude ~ 100 kyr cycle relative to the other five sites, which appears to be a regional feature unique to this record. The strong shift toward more negative $\delta^{18}\text{O}$ values at Site 1264 around 22.7 Ma results in reduced gradients between Site 1264 and the Pacific and Southern Ocean sites (Figure 9) and is associated with variability on 400 kyr timescales, coinciding with the termination phase of the transient glaciation across the OMT.

Comparing the short-term smooths between 22.6 and 22.9 Ma (Figure 7), $\delta^{18}\text{O}$ values at Site 1264 decrease compared to values earlier in the record between 21.9 Ma and 22.6 Ma and return to almost late Oligocene baseline values. The other five sites do not show a similar return to pre-OMT values, although Sites 926 and 929 also exhibit a decrease in values directly after the termination comparative to the youngest part of the record [Zachos *et al.*, 2001]. These comparatively low $\delta^{18}\text{O}$ values at Site 1264 appear untypical compared to the other early Miocene records. A slight return toward warmer conditions after the OMT recovery phase has been noted in previous studies [Zachos *et al.*, 2001; Lear *et al.*, 2004; Mawbey and Lear, 2013; Mudelsee *et al.*, 2014], suggesting a nonlinear and dynamic response present in the climate system [Zachos *et al.*, 2001]. This signal could be particularly prominent at Site 1264 due to more positive late Oligocene $\delta^{18}\text{O}$ values at Site 1264, which suggest colder/more saline bottom water conditions, relative to the other five sites. Site 1264 consistently has the most positive (baseline) $\delta^{18}\text{O}$ values of all six sites, and during the OMT, the other sites move toward the more positive (colder/more saline) $\delta^{18}\text{O}$ values at Site 1264 (Figure 9).

The maximum $\delta^{13}\text{C}$ values occur at all six sites ~ 30 kyr after the peak $\delta^{18}\text{O}$ values of the OMT, due to a global shift in the carbon cycle either triggered by or coincident with the expansion of the Antarctic Ice Sheet [Hodell and Woodruff, 1994; Diester-Haass *et al.*, 2011]. We calculated the relative change in $\delta^{13}\text{C}$ on the long-term smooths across the OMT for all six sites, relative to a baseline determined by averaging $\delta^{13}\text{C}$ values between 23.30 and 23.55 Ma. Across the glaciation, the range in relative amplitudes in the long-term $\delta^{13}\text{C}$ smooths between all six sites is minor (0.3–0.5‰) (Figure 9). After this shift across the OMT, the $\delta^{13}\text{C}$ baseline is distinctly offset toward more positive values in all data sets (Figure 9), a $\delta^{13}\text{C}$ stable isotope feature previously described as the Oligocene-Miocene Carbon Maximum [Hodell and Woodruff, 1994]. The long- and short-term smoothed data sets in the $\delta^{13}\text{C}$ record show the clear imprint of the long-period eccentricity forcing prior to and during the OMT (Figures 6 and 8). The strong response at the 400 kyr frequency seen in the $\delta^{13}\text{C}$ record is a consistent global feature of climate during the Oligocene and Miocene [Zachos *et al.*, 2001; Wade and Pälike, 2004; Pälike *et al.*, 2006a; Holbourn *et al.*, 2013, 2015].

5.3. Isotopic Gradients Between Sites

On an intrabasin scale, the offset in $\delta^{18}\text{O}$ between Sites U1334 and 1218 on astronomical timescales is small at 0.1‰, although the offset increases across the OMT (Figure 9). The similarity between the Pacific sites is unsurprising, as they are geographically close and from similar water depths. Preservation issues can be discounted as an explanation for the difference between the sites across the OMT, as foraminifera from Site 1218 have very good preservation across this time period [Lyle *et al.*, 2002; Edgar *et al.*, 2013]. The offset is within the limit suggested to account for different laboratory practices [Ostermann and Currie, 2002], but this does not explain an increase in the offset across the OMT. Either Site 1218 does not record the full extent of the coldest points during the OMT or in the equatorial Pacific, local variation exists in bottom water temperatures based on depth.

The long-term $\delta^{18}\text{O}$ SiZer smooths (Figure 9) indicate that the six records fall into two distinct groups. The equatorial Atlantic Sites 926 and 929 form one group, which is offset from the other four high-resolution records to consistently lighter $\delta^{18}\text{O}$ values, indicating that the seafloor at these equatorial Atlantic sites was bathed within relatively warm and/or a $\delta^{18}\text{O}$ -depleted water mass [Billups *et al.*, 2002]. Sites 926 and 929 are relatively constantly offset by ~ 1 ‰ from the equatorial Pacific Sites U1334 and 1218. The offset between the lighter $\delta^{18}\text{O}$ values in the equatorial Atlantic and the heavier $\delta^{18}\text{O}$ values equatorial Pacific could be related to temperature, suggesting equatorial Pacific bottom waters were colder than equatorial Atlantic

bottom waters. This supports previous suggestions of the existence of a warmer deep water mass present in the North Atlantic across the OMT [Woodruff and Savin, 1989; Billups et al., 2002].

The second group of $\delta^{18}\text{O}$ records consists of the sub-Antarctic Southern Ocean Site 1090, the two Pacific Sites 1218 and U1334, and the southeast Atlantic Site 1264, although 1264 exhibits some differences in $\delta^{18}\text{O}$ values from the other three sites. Sites 1218, 1264, and U1334 bear a close similarity to Site 1090, suggesting an Antarctic-sourced water mass was present at all three sites. Site 1264 consistently has the most positive $\delta^{18}\text{O}$ values, a surprising result given that it is the shallowest site. One possible explanation is the presence of a more saline (high $\delta^{18}\text{O}$) water mass at Site 1264. During the glaciation at the OMT, gradients between Site 1264 and the Southern Ocean and Pacific sites (1090, 1218, and U1334) reduce and remain smaller into the early Miocene.

Deep ocean $\delta^{13}\text{C}$ gradients between basins are negligible across the OMT, regardless of changes in ocean circulation. The low gradients in $\delta^{13}\text{C}$ are attributed to a generally low-nutrient ocean [Delaney and Boyle, 1987; Wright et al., 1991; Billups et al., 2002]. However, we observe some differences between the sites. Carbon isotope gradients between the deeper Sites U1334, 1218, 926, 929, and 1090 are small, but Site 1264 is offset from the other sites by $\sim +0.5\text{‰}$ (Figure 9). The difference in $\delta^{13}\text{C}$ gradients between Site 1264 and the other five sites is most likely due to its shallower water depth location [Liebrand et al., 2011]. In this respect, it is interesting to note that Site 1264 revealed a weak imprint of obliquity in both stable isotope records across the OMT [Liebrand et al., 2011] compared to the equatorial, though deep water, Sites 926 and 929 [Flower et al., 1997; Paul et al., 2000] (Figure 9). Our findings at Site U1334 confirm a distinct obliquity imprint in both $\delta^{18}\text{O}$ and $\delta^{13}\text{C}$ during the OMT in the deep waters of the Pacific (Figure 6), indicating that most likely the obliquity signal is transferred from high latitudes (i.e., Antarctica) to the equator primarily through deep water masses. Alternatively, Site 1264 has low sedimentation rates, which could distort the preservation of higher frequency astronomical cycles and lead to a weak obliquity signal. After the OMT, $\delta^{13}\text{C}$ values at all sites increase and show greater variability, and the imprint of the 400 kyr eccentricity cycle is less easy to distinguish; in particular, the Pacific/Southern Ocean sites have a more variable $\delta^{13}\text{C}$ signal.

6. Conclusions

We have constructed new high-resolution (~ 3 kyr) benthic foraminiferal stable isotope records in the equatorial Pacific basin and compare these data sets to other high-resolution records from different ocean basins to evaluate global and regional climate variability across the OMT. We find that the benthic foraminiferal stable isotope records from IODP Site U1334 are remarkably consistent with previously published records, confirming the global nature of the $\delta^{18}\text{O}$ signal in the Pacific. Peak $\delta^{18}\text{O}$ values associated with the OMT (i.e., Mi-1 oxygen isotope zone) occur in the latest Oligocene prior to the Oligocene/Miocene boundary. Gradients between sites suggest that the high-resolution records fall into two groups, dominated by two different water masses, supporting previous suggestions of the existence of deep water formation in the North Atlantic during the Oligocene-Miocene. We find pervasive cyclicity at long- and short-period eccentricity frequencies (400 and ~ 100 kyr) and confirm a distinct obliquity imprint (41 kyr) present in the stable isotope records at Site U1334. We find an offset in $\delta^{18}\text{O}$ records between the deep equatorial Atlantic and deep equatorial Pacific basins, which suggests a temperature gradient is present between the equatorial Pacific bottom waters and the equatorial Atlantic bottom waters across the OMT.

References

- Billups, K., J. E. T. Channell, and J. C. Zachos (2002), Late Miocene through early Pliocene deep water circulation and climate change viewed from the sub-Antarctic South Atlantic, *Palaeogeogr. Palaeoclimatol. Palaeoecol.*, *185*, 287–307.
- Billups, K., H. Pälike, J. E. T. Channell, J. C. Zachos, and N. J. Shackleton (2004), Astronomic calibration of the late Oligocene through early Miocene geomagnetic polarity time scale, *Earth Planet. Sci. Lett.*, *224*, 33–44, doi:10.1016/j.epsl.2004.05.004.
- Bohaty, S. M., J. C. Zachos, and M. L. Delaney (2012), Foraminiferal Mg/Ca evidence for Southern Ocean cooling across the Eocene–Oligocene transition, *Earth Planet. Sci. Lett.*, *317*, 251–261.
- Bowles, J. (2006), Data report: revised magnetostratigraphy and magnetic mineralogy of sediments from Walvis Ridge, Leg 208, Ocean Drill. Program, College Station, Tex.
- Brown, R. E., L. D. Anderson, E. Thomas, and J. C. Zachos (2011), A core-top calibration of B/Ca in the benthic foraminifers *Nuttallides umbonifera* and *Oridorsalis umbonatus*: A proxy for Cenozoic bottom water carbonate saturation, *Earth Planet. Sci. Lett.*, *310*(3), 360–368, doi:10.1016/j.epsl.2011.08.023.
- Channell, J. E. T., S. Galeotti, E. E. Martin, K. Billups, H. Scher, and J. S. Stoner (2003), Eocene to Miocene magnetic, bio- and chemo-stratigraphy at ODP Site 1090 (sub-Antarctic South Atlantic), *Geol. Soc. Am. Bull.*, *115*, 607–623.

Acknowledgments

This research used samples provided by the Integrated Ocean Drilling Program (IODP), collected by the staff, crew, and scientists of IODP Expedition 320/321. We thank Dominika Kasjanuk, Arnold van Dijk, Maxim Krasnoperov, and Jan Drenth for laboratory assistance and Vittoria Lauretano, Stefanie Kaboth, Frits Hilgen, Heiko Pälike, and Steve Bohaty for useful discussions. We thank Ann Holbourn and two anonymous reviewers for constructive and helpful reviews. This research was supported by NWO VICI grant [865.10.001] awarded to L.J. Lourens. A. Sluijs thanks the European Research Council (ERC) under the European Union Seventh Framework Program for ERC Starting grant 259627. B. Wade was supported by the Natural Environment Research Council reference NE/G014817. This work was carried out under the program of the Netherlands Earth System Science Centre (NESSC). Data are available in the supporting information tables and online through Pangaea.

- Channell, J. E. T., C. Ohneiser, Y. Yamamoto, and M. S. Kesler (2013), Oligocene-Miocene magnetic stratigraphy carried by biogenic magnetite at sites U1334 and U1335 (equatorial Pacific Ocean), *Geochim. Geophys. Geosyst.*, *14*, 265–282, doi:10.1029/2012GC004429.
- Chaudhuri, P., and J. S. Marron (1999), SiZer for exploration of structures in curves, *J. Am. Stat. Assoc.*, *94*(447), 807–823.
- Coxall, H. K., and P. A. Wilson (2011), Early Oligocene glaciation and productivity in the eastern equatorial Pacific: Insights into global carbon cycling, *Paleoceanography*, *26*, PA2221, doi:10.1029/2010PA002021.
- De Boer, B., R. S. W. van de Wal, R. Bintanja, L. J. Lourens, and E. Tuentler (2010), Cenozoic global ice volume and temperature simulations with 1-D ice-sheet models forced by benthic $\delta^{18}\text{O}$ records, *Ann. Glaciol.*, *51*(55), 23–33.
- De Boer, B., R. S. W. Van de Wal, L. J. Lourens, and R. Bintanja (2012), Transient nature of the Earth's climate and the implications for the interpretation of benthic $\delta^{18}\text{O}$ records, *Palaeogeogr. Palaeoclimatol. Palaeoecol.*, *335*–336, 4–11.
- Delaney, M. L., and E. A. Boyle (1987), Cd/Ca in late Miocene benthic foraminifera and changes in the global organic carbon budget, *Nature*, *330*, 156–159.
- Diester-Haass, L., K. Billups, and K. Emeis (2011), Enhanced paleoproductivity across the Oligocene/Miocene boundary as evidenced by benthic foraminiferal accumulation rates, *Palaeogeogr. Palaeoclimatol. Palaeoecol.*, *302*, 464–473, doi:10.1016/j.palaeo.2011.02.006.
- Diz, P., C. Barras, E. Geslin, G. J. Reichert, E. Metzger, F. Jorissen, and J. Bijma (2012), Incorporation of Mg and Sr and oxygen and carbon stable isotope fractionation in cultured *Ammonia tepida*, *Mar. Micropaleontol.*, *92*, 16–28.
- Edgar, K. M., H. Pälike, and P. A. Wilson (2013), Testing the impact of diagenesis on the $\delta^{18}\text{O}$ and $\delta^{13}\text{C}$ of benthic foraminiferal calcite from a sediment burial depth transect in the equatorial Pacific, *Paleoceanography*, *28*, 468–480, doi:10.1002/palo.20045.
- Elderfield, H., M. Greaves, S. Barker, I. R. Hall, A. Tripathi, P. Ferretti, S. Crowhurst, L. Booth, and C. Daunt (2010), A record of bottom water temperature and seawater $\delta^{18}\text{O}$ for the Southern Ocean over the past 440 kyr based on Mg/Ca of benthic foraminiferal *Uvigerina* spp, *Quat. Sci. Rev.*, *29*, 160–169, doi:10.1016/j.quascirev.2009.07.013.
- Fairbanks, R. G., and R. K. Matthews (1978), The marine oxygen isotope record in Pleistocene coral, Barbados, West Indies, *Quat. Res.*, *10*(2), 181–196.
- Flower, B. P., J. C. Zachos, and H. Paul (1997), Milankovitch-scale variability recorded near the Oligocene/Miocene boundary: Hole 929A, in *Proceedings of ODP Science Research*, vol. 154, edited by N. J. Shackleton et al., pp. 433–439, Ocean Drill. Program, College Station, Tex.
- Friedrich, O., G. Schmiedl, and H. Erlenkeuser (2006), Stable isotope composition of Late Cretaceous benthic foraminifera from the southern South Atlantic: Biological and environmental effects, *Mar. Micropaleontol.*, *58*(2), 135–157.
- Hilgen, F. J., L. J. Lourens, and J. A. Van Dam (2012), The Neogene period, in *The Geologic Time Scale*, vol. 2, pp. 923–978, Elsevier, Boston, Mass.
- Hodell, D. A., and F. Woodruff (1994), Variations in the strontium isotopic ratio of seawater during the Miocene: Stratigraphic and geochemical implications, *Paleoceanography*, *9*, 405–426.
- Holbourn, A., W. Kuhnt, S. Clemens, W. Prell, and N. Andersen (2013), Middle to late Miocene stepwise climate cooling: Evidence from a high-resolution deep-water isotope curve spanning 8 million years, *Paleoceanography*, *28*, 688–699, doi:10.1002/2013PA002538.
- Holbourn, A., W. Kuhnt, K. G. Kochhann, N. Andersen, and K. S. Meier (2015), Global perturbation of the carbon cycle at the onset of the Miocene Climatic Optimum, *Geology*, *43*(2), 123–126.
- Hoogakker, B., H. Elderfield, K. Oliver, and S. Crowhurst (2010), Benthic foraminiferal oxygen isotope offsets over the last glacial-interglacial cycle, *Paleoceanography*, *25*, PA4229, doi:10.1029/2009PA001870.
- Katz, M. E., D. R. Katz, J. D. Wright, K. G. Miller, D. K. Pak, N. J. Shackleton, and E. Thomas (2003), Early Cenozoic benthic foraminiferal isotopes: Species reliability and interspecies correction factors, *Paleoceanography*, *18*(2), 1024, doi:10.1029/2002PA000798.
- Lanci, L., J. M. Pares, J. E. T. Channell, and D. V. Kent (2004), Miocene magnetostratigraphy from equatorial Pacific sediments (ODP Site 1218, Leg 199), *Earth Planet. Sci. Lett.*, *226*(1), 207–224.
- Lanci, L., J. M. Pares, J. E. Channell, and D. V. Kent (2005), Oligocene magnetostratigraphy from equatorial Pacific sediments (ODP Sites 1218 and 1219, Leg 199), *Earth Planet. Sci. Lett.*, *237*(3), 617–634.
- Lear, C. H., Y. Rosenthal, H. K. Coxall, and P. A. Wilson (2004), Late Eocene to early Miocene ice-sheet dynamics and the global carbon cycle, *Paleoceanography*, *19*, PA4015, doi:10.1029/2004PA001039.
- Liebrand, D., L. Lourens, D. A. Hodell, B. de Boer, R. S. W. van der Wal, and H. Pälike (2011), Antarctic ice sheet and oceanographic response to eccentricity forcing in the early Miocene, *Clim. Past*, *7*, 869–880.
- Lisiecki, L. E., and P. A. Lisiecki (2002), Application of dynamic programming to the correlation of paleoclimate records, *Paleoceanography*, *17*(4), 1049, doi:10.1029/2001PA000733.
- Lyle, M., et al. (2002), *Proceeding of the ODP, Initial Rep.*, vol. 199, Ocean Drilling Program, College Station, Tex., doi:10.2973/odp.proc.ir.199.2002.
- Lyle, M., J. Barron, T. J. Bralower, M. Huber, A. Olivarez Lyle, A. C. Ravelo, D. K. Rea, and P. A. Wilson (2008), Pacific Ocean and Cenozoic evolution of climate, *Rev. Geophys.*, *46*, RG2002, doi:10.1029/2005RG000190.
- Lyle, M., H. Pälike, H. Nishi, I. Raffi, K. Gamage, A. Klaus, and the IODP Expeditions 320/321 Science Party (2010), The Pacific Equatorial Age Transect, IODP Expeditions 320 and 321: Building a 50-million-year-long environmental record of the equatorial Pacific Ocean, *Sci. Drill.*, *9*, 4–15, doi:10.2204/iodp.sd.9.01.2010.
- Mawbey, E. M., and C. H. Lear (2013), Carbon cycle feedbacks during the Oligocene-Miocene transient glaciation, *Geology*, doi:10.1130/G34422.1.
- McConnaughey, T. (1989a), ^{13}C and ^{18}O isotopic disequilibrium in biological carbonates: I. Patterns, *Geochim. Cosmochim. Acta*, *53*, 151–162.
- McConnaughey, T. (1989b), ^{13}C and ^{18}O isotopic disequilibrium in biological carbonates: II. In vitro simulation of kinetic isotope effects, *Geochim. Cosmochim. Acta*, *53*, 163–171.
- McConnaughey, T. A., J. Burdett, J. F. Whelan, and C. K. Paull (1997), Carbon isotopes in biological carbonates: Respiration and photosynthesis, *Geochim. Cosmochim. Acta*, *61*, 611–622.
- Miller, K. G., J. Wright, and R. Fairbanks (1991), Unlocking the icehouse: Oligocene-Miocene oxygen isotopes, eustasy and margin erosion, *J. Geophys. Res.*, *96*, 6829–6848, doi:10.1029/90JB02015.
- Mudelsee, M., T. Bickert, C. H. Lear, and G. Lohmann (2014), Cenozoic climate changes: A review based on time series analysis of marine benthic $\delta^{18}\text{O}$ records, *Rev. Geophys.*, *52*, 333–374, doi:10.1002/2013RG000440.
- Ostermann, D. R., and W. B. Curry (2000), Calibration of stable isotopic data: An enriched $\delta^{18}\text{O}$ standard used for source gas mixing detection and correction, *Paleoceanography*, *15*(3), 353–360.
- Paillard, D., L. Labeyrie, and P. Yiou (1996), Macintosh program performs time-series analysis, *Eos Trans. AGU*, *77*, 379, doi:10.1029/96EO00259.
- Pälike, H., J. Frazier, and J. C. Zachos (2006a), Extended orbitally forced palaeoclimatic records from the equatorial Atlantic Ceara Rise, *Quat. Sci. Rev.*, *25*, 3138–3149.
- Pälike, H., R. N. Norris, J. Herrle, P. A. Wilson, H. K. Coxall, C. H. Lear, N. J. Shackleton, A. K. Tripathi, and B. S. Wade (2006b), The heartbeat of the Oligocene climate system, *Science*, *314*, 1894–1898, doi:10.1126/science.1133822.

- Pälike, H., M. W. Lyle, H. Nishi, I. Raffi, K. Gamage, A. Klaus, and the Expedition 320/321 Scientists (2010), *Proceedings of the Integrated Ocean Drilling Program*, vol. 320/321, Integrated Ocean Drill. Program Manage. Int., Tokyo.
- Pälike, H., et al. (2012), A Cenozoic record of the equatorial Pacific carbonate compensation depth, *Nature*, 488(7413), 609–614.
- Paul, H. P., J. C. Zachos, B. P. Flower, and A. Tripathi (2000), Orbitally induced climate and geochemical variability across the Oligocene/Miocene boundary, *Paleoceanography*, 15, 471–485.
- Pekar, S. F., N. Christie-Blick, M. A. Kominz, and K. G. Miller (2002), Calibration between eustatic estimates from backstripping and oxygen isotopic records for the Oligocene, *Geology*, 30(10), 903–906.
- Schlitzer, R. (2010), Ocean Data View 4, version 4.3.6. [Available at <http://odv.awi.de>.]
- Schmiedl, G., and A. Mackensen (2006), Multispecies stable isotopes of benthic foraminifers reveal past changes of organic matter decomposition and deepwater oxygenation in the Arabian Sea, *Paleoceanography*, 21, PA4213, doi:10.1029/2006PA001284.
- Schmiedl, G., M. Pfeilsticker, C. Hemleben, and A. Mackensen (2004), Environmental and biological effects on the stable isotope composition of recent deep-sea benthic foraminifera from the western Mediterranean Sea, *Mar. Micropaleontol.*, 51(1), 129–152, doi:10.1016/j.marmicro.2003.10.001.
- Shackleton, N. J., M. Hall, and A. Boersma (1984), Oxygen and carbon isotope data from Leg 74 foraminifers, *Initial Rep. Deep Sea Drill. Proj.*, 74, 599–612.
- Shackleton, N. J., M. A. Hall, I. Raffi, L. Tauxe, and J. C. Zachos (2000), Astronomical calibration age for the Oligocene/Miocene boundary, *Geology*, 28(5), 447–450.
- Shevenell, A. E., and J. P. Kennett (2007), Cenozoic Antarctic cryosphere evolution: Tales from deep-sea sedimentary records, *Deep Sea Res., Part II*, 54(21), 2308–2324.
- Thornalley, D. J., H. A. Bauch, G. Gebbie, W. Guo, M. Ziegler, S. M. Bernasconi, S. Barker, L. Skinner, and J. Yu (2015), A warm and poorly ventilated deep Arctic Mediterranean during the last glacial period, *Science*, 349(6249), 706–710.
- Torrence, C., and G. P. Compo (1998), A practical guide to wavelet analysis, *Bull. Am. Meteorol. Soc.*, 79, 61–78.
- Uchikawa, J., and R. E. Zeebe (2010), Examining possible effects of seawater pH decline on foraminiferal stable isotopes during the Paleocene-Eocene Thermal Maximum, *Paleoceanography*, 25, PA2216, doi:10.1029/2009PA001864.
- Vandenbergh, N., F. J. Hilgen, and R. P. Speijer (2012), The Paleogene period, in *The Geologic Time Scale*, vol. 2012, pp. 855–921, Elsevier, Boston, Mass.
- Wade, B. S., and H. Pälike (2004), Oligocene climate dynamics, *Paleoceanography*, 19, PA4019, doi:10.1029/2004PA001042.
- Westerhold, T., et al. (2012), Revised composite depth scales and integration of IODP Sites U1331–U1334 and ODP Sites 1218–1220, in *Proceedings of the Integrated Ocean Drilling Program*, vol. 320/321, edited by H. Pälike et al., Integrated Ocean Drill. Program Manage. Int., College Station, Tex.
- Woodruff, F., and S. M. Savin (1989), Miocene deepwater oceanography, *Paleoceanography*, 4, 87–140.
- Wright, J. D., K. G. Miller, and R. G. Fairbanks (1991), Evolution of modern deep water circulation: Evidence from the late Miocene Southern Ocean, *Paleoceanography*, 6, 275–290.
- Zachos, J. C., B. P. Flower, and H. A. Paul (1997), Orbitally paced climate oscillations across the Oligocene/Miocene boundary, *Nature*, 388, 567–570.
- Zachos, J. C., N. J. Shackleton, J. S. Revenaugh, H. Pälike, and B. P. Flower (2001), Climate response to orbital forcing across the Oligocene–Miocene boundary, *Science*, 292, 274–278.
- Zeebe, R. E. (1999), An explanation of the effect of seawater carbonate concentration on foraminiferal oxygen isotopes, *Geochim. Cosmochim. Acta*, 63(13), 2001–2007.